Conversion of a Signal into Forces for Axon Outgrowth through Pak1-mediated Shootin1 Phosphorylation

Michinori Toriyama[1], Satoshi Kozawa[2], Yuichi Sakumura[1,3] and Naoyuki Inagaki[1]*

[1]Laboratory of Neuronal Cell Morphogenesis, Graduate School of Biological Sciences, Nara Institute of Science and Technology, Ikoma, Nara 630-0192, Japan.

[2]Laboratory of Mathematical Informatics, Graduate School of Information Science, Nara Institute of Science and Technology, Ikoma, Nara 630-0192, Japan.

[3]Biological Systems Design Laboratory, School of Information Science and Technology, Aichi Prefectural University, Nagakute, Aichi 480-1198, Japan.

*To whom correspondence should be addressed. E-mail: ninagaki@bs.naist.jp

Summary

Soluble guidance cues can direct cellular protrusion and migration by modulating adhesion and cytoskeletal dynamics. Actin filaments (F-actins) polymerize at the leading edge of motile cells and depolymerize proximally [1, 2]; this, together with myosin II activity, induces retrograde flow of F-actins [3-5]. It has been proposed that the traction forces underlying cellular motility may be regulated by the modulation of coupling efficiency between F-actin flow and the extracellular substrate via "clutch" molecules [6-10]. However, how cell signaling controls the coupling efficiency remains unknown. Shootin1 functions as a linker molecule that couples F-actin retrograde flow and the substrate at neuronal growth cones to promote axon outgrowth [11]. Here, we show that shootin1 is located at a critical interface, transducing a chemical signal into traction forces for axon outgrowth. We found that a chemoattractant, netrin-1, positively regulates traction forces at axonal growth cones via Pak1-mediated shootin1 phosphorylation. This phosphorylation enhanced the interaction between shootin1 and F-actin retrograde flow, thereby promoting F-actin-substrate coupling, force generation, and concomitant filopodium extension and axon outgrowth. These results suggest that dynamic actin-substrate coupling can transduce chemical signals into mechanical forces to control cellular motility, and provide a molecular-level description of how this transduction may occur.

Results and Discussion

To analyze the regulation of mechanical forces in motile cells, we studied axonal growth cones of cultured rat hippocampal neurons. Recent experiments have shown that directional traction forces are generated by growth cones [12, 13]. In addition, growth cones respond to netrin-1, thereby promoting axon outgrowth [14, 15]. Consistent with previous reports [14, 16, 17], stimulation of hippocampal neurons by netrin-1 bath application promoted activation of the Rho family small GTPases Cdc42 and Rac1 (Figure S1A), filopodium extension (Figure S1B), and axon outgrowth (Figure S1C). A recent study showed that substrate-bound netrin-1 can induce the generation of traction forces by spinal commissural neurons [18]. However, we could not observe a comparable promotion of axon outgrowth by netrin-1 pre-absorbed to the substrate (Figure S1D), suggesting that the effects observed here were mediated mainly by soluble netrin-1. To test the possibility that netrin-1 might regulate traction forces for filopodium extension and axon outgrowth, we measured the traction forces generated by axonal growth cones using traction force microscopy [12, 19]. Hippocampal neurons were cultured on L1-CAM-coated polyacrylamide gels embedded with 200-nm fluorescent beads. Traction forces under the growth cones were monitored by visualizing force-induced deformation of the elastic substrate, which is reflected by displacement of the beads from their original positions. As reported previously [12], the reporter beads under the growth cones moved dynamically toward the center in a “load-and-fail” manner (Figure 1A; Movie S1). Directional movement of the beads was detected mainly under the peripheral region of the growth cones, where the distal part of F-actin flow was observed (Figure S1E). As the

displacement of individual beads showed dynamic fluctuation, we calculated average stress and peak stress under the growth cones during 125-sec observations. Consistent with the previous study [12, 13], histogram analysis showed a wide range of average and peak stresses (Figures 1B and 1C). However, statistical analysis revealed that both increased significantly after netrin-1 stimulation (Figures 1B and 1C). We also analyzed the orientation and the magnitude of the vector of the net force under the growth cones (Figure 1D). The net force was oriented toward the rear of the growth cones, consistent with the notion that it serves as the traction force for axon outgrowth. The magnitude of the net force increased markedly after netrin-1 treatment, whereas its orientation did not change significantly, indicating that the external signal netrin-1 positively regulates traction forces at growth cones.

To elucidate the molecular mechanism by which netrin-1 enhances these traction forces, we focused on p21-activated kinase 1 (Pak1) [20] and shootin1 [21]. Pak1 is a downstream effector kinase of Cdc42 and Rac1, and is involved in axon outgrowth and cell migration [22, 23]. Shootin1 functions as a linker molecule to promote axon outgrowth by coupling F-actin retrograde flow and the extracellular substrate, via L1-CAM, at axonal growth cones [11]. By mass spectrometry, we identified several possible phosphorylation sites in shootin1; two of them, Ser101 and Ser249, were conserved consensus phosphorylation sites for Pak1 (Figure S2A). *In vitro* kinase assays demonstrated that Pak1 phosphorylates shootin1 directly at both Ser101 and Ser249 (Figures S2B and S2C). We raised antibodies that recognize the phosphorylated residue at each site to analyze their intracellular phosphorylation status. In cultured neurons, shootin1 phosphorylation at both

Ser101 and Ser249 increased markedly upon ectopic expression of a constitutively active Pak1 (CA-Pak1), while inhibition of endogenous Pak1 by its dominant negative form (DN-Pak1, AID) reduced the phosphorylation levels of both residues (Figure S2D). Expression of constitutively active Cdc42 and Rac1 also promoted shootin1 phosphorylation, but that of RhoA did not (Figure S2E). Furthermore, netrin-1 stimulation increased the phosphorylation of shootin1 at both sites (Figure 2A), and this was also abolished when endogenous Pak1 was inhibited by DN-Pak1 (Figure 2B). Thus, netrin-1, via activation of Cdc42 and Rac1, up-regulates Pak1-mediated shootin1 phosphorylation.

Immunocytochemical analysis showed that phosphorylated shootin1 accumulated to a high level in filopodia and lamellipodia of axonal growth cones, where F-actin retrograde flow and traction forces were observed [11, 12] (Figure 2C). To examine the correlation between the shootin1 phosphorylation and its interaction with F-actin, we performed fluorescent speckle microscopy, which can detect molecules attached to F-actin retrograde flow as moving speckles [11, 24]. We produced phosphomimic shootin1 (shootin1-DD), in which both Ser101 and Ser249 were replaced by aspartate, and unphosphorylated shootin1 (shootin1-AA), where these residues were replaced by alanine. Neurons expressing EGFP-labeled wild-type shootin1 (shootin1-WT) and shootin1-DD displayed fluorescent speckles which moved retrogradely at the peripheral region of growth cones (Figure 2D; Movie S2). The velocities of shootin1-WT and shootin1-DD retrograde flow were 3.6 ± 0.9 μm/min (mean ± SD, n = 25) and 3.4 ± 0.9 μm/min (mean ± SD, n = 31), respectively. Their speed was similar to that previously reported for F-actin [11], indicating that wild-type and phosphomimic shootin1 interact with F-actin retrograde flow.

In contrast, EGFP-labeled unphosphorylated shootin1 showed a diffuse distribution throughout growth cones, without forming retrograde speckle signals (Figure 2D; Movie S2). Furthermore, inhibition of Pak1-mediated shootin1 phosphorylation by DN-Pak1 significantly decreased the localization of endogenous shootin1 to axonal growth cones without affecting the amount of F-actin (Figure S2F), thereby suggesting its dissociation from F-actin. Together, these results suggest that Pak1-mediated phosphorylation enhances the association of shootin1 with F-actin retrograde flow at growth cones.

We next examined whether the dynamic interaction between shootin1 and F-actin flow can regulate F-actin–substrate coupling (clutch engagement [2, 10]) and the transmission of traction forces. The F-actin retrograde flow is driven by both myosin II activity and actin polymerization at growth cones [5]. Clutch engagement is thought to transmit the forces of F-actin retrograde flow to the substrate; this engagement would also reduce the speed of the F-actin retrograde flow, converting actin polymerization into protrusion of the leading edge [2, 10]. To examine the involvement of the Pak1-regulated interaction between shootin1 and F-actin flow in clutch engagement, we analyzed F-actin retrograde flow by speckle microscopy [11, 24]: the flow velocity was monitored by kymograph analysis of mRFP-actin speckles in filopodia and lamellipodia (Figure 3A; Movie S3). In control growth cones, actin speckles moved retrogradely at 4.4 ± 1.1 μm/min (mean ± SD, n = 188), as reported previously [11]. Consistent with the role of shootin1 as a linker molecule, reduction of shootin1 expression by RNAi increased the velocity of F-actin flow (Figures 3A and 3B), reflecting increased slippage of the clutch engagement (Figures S3A; see also Supplemental Results and S3B) [2, 10]. Netrin-1

stimulation significantly decreased the velocity of F-actin flow, yet increased it when shootin1 expression was reduced (Figures 3A and 3B), suggesting that netrin-1 promotes clutch engagement that is dependent on shootin1 (for a detailed explanation for the reversal effects of netrin-1, see Supplemental Discussion and Figure S3A and S3C). Consistent with the involvement of shootin1 in netrin-1-mediated clutch engagement, shootin1 RNAi also decreased the netrin-1-mediated promotion of traction forces at growth cones (Figure 3C). Inhibition of endogenous Pak1 activity by DN-Pak1 increased the velocity of F-actin flow (Figure 3D), and decreased the traction forces (Figure 3E), indicating that Pak1 contributes to clutch engagement and force transmission. Furthermore, co-expression of the phosphomimic shootin1-DD rescued the effects of DN-Pak1, whereas co-expression of shootin1-WT partially rescued the effect of DN-Pak1 on peak stress but not on F-actin flow or average stress (Figures 3D and 3E). Myosin II activity in growth cones promotes F-actin retrograde flow [5] and is involved in netrin-1-mediated growth cone collapse and axon repulsion of cranial motor neurons [25]. In addition, L1-CAM on the growth cone membrane constitutes a component of the clutch system [11]. However, netrin-1 stimulation, Pak1 inhibition or shootin1 RNAi did not alter myosin II activity or L1-CAM surface expression (Figures S3D and S3E). It is therefore unlikely that netrin-1 up-regulates the traction forces at growth cones through the regulation of myosin II activity or L1-CAM surface expression. Together, these data suggest that netrin-1- and Pak1-mediated shootin1 interaction with F-actin flow promotes clutch engagement and concomitant formation of traction forces at axonal growth cones.

Finally, we asked whether filopodium extension and axon outgrowth depend on

the clutch engagement and force transmission regulated by Pak1-mediated shootin1 phosphorylation. In agreement with previous work [11], inhibition of clutch engagement by shootin1 RNAi reduced the filopodium and axon lengths (Figures 4A and S4A). In addition, this treatment significantly decreased netrin-1-promoted filopodium extension and axon outgrowth (Figures 4A and S4A). Expression of RNAi-refractory wild-type and phosphomimic shootin1 rescued the reduction of filopodium and axon length by shootin1 RNAi, but unphosphorylated shootin1 had no effect (Figure 4B and S4B). Furthermore, a decrease in clutch engagement by DN-Pak1 significantly suppressed filopodium extension and axon outgrowth, and this effect was rescued by expression of the phosphomimic shootin1, but not by wild-type shootin1 (Figure 4C and S4C). Thus, clutch engagement and force transmission enhanced by Pak1-mediated shootin1 phosphorylation up-regulates filopodium extension and axon outgrowth.

Together, these results show that the dynamic interaction between shootin1 and F-actin, which is regulated by Pak1-mediated shootin1 phosphorylation, transduces a chemical signal into traction forces for axon outgrowth (black, blue, and green arrows, Figure 4D). Pak1 is known to regulate a variety of other downstream molecules [26]. However, the effects of DN-Pak1 on F-actin flow (Figure 3D), traction force (Figure 3E), filopodium extension (Figure S4C), and axon outgrowth (Figure 4C) were all rescued by the phosphomimic shootin1, indicating a core role for shootin1 phosphorylation by Pak1 in these Pak1-mediated processes. Cdc42 and Rac1, which are located upstream of Pak1, are known to play key roles in the regulation of cell motility under various external signals [1, 27, 28]. It is notable that Cdc42 and Rac1 promote actin polymerization at the leading edge

[1, 2, 29-31], which is required to induce F-actin retrograde flow [1, 2, 5] (red arrows, Figure 4D). These two processes may work coordinately to effectively regulate mechanical forces for cell motility.

The present model may explain axon guidance mediated by the DCC (deleted in colorectal cancer) and UNC-5 families of netrin-1 receptors [32, 33]. DCC mediates activation of molecules including Cdc42, Rac1 and Pak1 [16] and promotes axon outgrowth and attraction, whereas axon repulsion involves the activation of UNC-5, RhoA, Rho-kinase, myosin light chain kinase and myosin II [25]. In the case of netrin-1-induced axon attraction, asymmetric activation of DCC on growth cones would lead to the local activation of Cdc42, Rac1 and Pak1. This would in turn promote shootin1 phosphorylation, clutch engagement and an increase in traction force on the side of netrin-1 stimulation for axon attraction (Figure S4D). On the other hand, how UNC-5 and its downstream molecules may regulate traction force is more elusive. However, as RhoA is known to inhibit Rac1 [34], we expect that local activation of RhoA would inhibit clutch engagement and decrease traction force on the side of netrin-1 stimulation. This, together with myosin II activation, might effectively retract the stimulated side of growth cones and thus cause axon repulsion. We do not rule out the involvement of other molecules in coupling the actin filament flow to the substrate. Other pathways may also participate in the regulation of traction forces. In addition, the mechanical properties of the cellular substrates may influence the effect of netrin-1 signaling, in the same way as they are reported to modulate clutch coupling efficiency [12]. The details of how traction forces are regulated for axon attraction and repulsion remain important issues for future investigation.

Experimental Procedures

All relevant aspects of the experimental procedures were approved by the Institutional Animal Care and Use Committee of the Nara Institute of Science and Technology.

Supplemental Information

Supplemental Information includes Supplemental Results and Discussion, 4 Supplemental Figures, 3 Movies and Supplemental Experimental Procedures.

Acknowledgments

We thank M. Inagaki and L. Lim for Pak1 constructs, K. Kaibuchi for Cdc42, Rac1 and RhoA constructs, N. Yokota for mass spectrometry, S. Kai for data analysis, K. Ikeda, T. Sugiura, Y. Iwadate, and M. Kuwano for discussion, and T. Hakoshima and I. Smith for reviewing the manuscript. This research was supported in part by MEXT and JSPS KAKENHI Grant numbers 23111518, 23700448, 22500279, the Global COE Program at NAIST (MEXT), Osaka Medical Research Foundation for Incurable Diseases, and the NAIST Interdisciplinary Frontier Research Project.

References

1. Pollard, T.D., and Borisy, G.G. (2003). Cellular motility driven by assembly and disassembly of actin filaments. Cell *112*, 453-465.
2. Le Clainche, C., and Carlier, M.F. (2008). Regulation of actin assembly associated with protrusion and adhesion in cell migration. Physiol. Rev. *88*, 489-513.
3. Forscher, P., and Smith, S.J. (1988). Actions of cytochalasins on the organization of actin filaments and microtubules in a neuronal growth cone. J. Cell Biol. *107*, 1505-1516.
4. Katoh, K., Hammar, K., Smith, P.J., and Oldenbourg, R. (1999). Birefringence imaging directly reveals architectural dynamics of filamentous actin in living growth cones. Mol. Biol. Cell *10*, 197-210.
5. Medeiros, N.A., Burnette, D.T., and Forscher, P. (2006). Myosin II functions in actin-bundle turnover in neuronal growth cones. Nat. Cell Biol. *8*, 215-226.
6. Mitchison, T., and Kirschner, M. (1988). Cytoskeletal dynamics and nerve growth. Neuron *1*, 761-772.
7. Suter, D.M., and Forscher, P. (2000). Substrate-cytoskeletal coupling as a mechanism for the regulation of growth cone motility and guidance. J. Neurobiol. *44*, 97-113.
8. Hu, K., Ji, L., Applegate, K.T., Danuser, G., and Waterman-Storer, C.M. (2007). Differential transmission of actin motion within focal adhesions. Science *315*, 111-115.
9. Giannone, G., Mege, R.M., and Thoumine, O. (2009). Multi-level molecular clutches in motile cell processes. Trends Cell Biol. *19*, 475-486.
10. Lowery, L.A., and Van Vactor, D. (2009). The trip of the tip: understanding the growth cone machinery. Nat. Rev. Mol. Cell Biol. *10*, 332-343.
11. Shimada, T., Toriyama, M., Uemura, K., Kamiguchi, H., Sugiura, T., Watanabe, N., and Inagaki, N. (2008). Shootin1 interacts with actin retrograde flow and L1-CAM to promote axon outgrowth. J. Cell Biol. *181*, 817-829.
12. Chan, C.E., and Odde, D.J. (2008). Traction dynamics of filopodia on compliant substrates. Science *322*, 1687-1691.
13. Koch, D., Rosoff, W.J., Jiang, J., Geller, H.M., and Urbach, J.S. (2012). Strength in the periphery: growth cone biomechanics and substrate rigidity response in peripheral and central nervous system neurons. Biophys. J. *102*, 452-460.
14. Li, X., Gao, X., Liu, G., Xiong, W., Wu, J., and Rao, Y. (2008). Netrin signal transduction and the guanine nucleotide exchange factor DOCK180 in attractive signaling. Nat. Neurosci. *11*, 28-35.

15. Serafini, T., Kennedy, T.E., Galko, M.J., Mirzayan, C., Jessell, T.M., and Tessier-Lavigne, M. (1994). The netrins define a family of axon outgrowth-promoting proteins homologous to C. elegans UNC-6. Cell *78*, 409-424.

16. Shekarabi, M., Moore, S.W., Tritsch, N.X., Morris, S.J., Bouchard, J.F., and Kennedy, T.E. (2005). Deleted in colorectal cancer binding netrin-1 mediates cell substrate adhesion and recruits Cdc42, Rac1, Pak1, and N-WASP into an intracellular signaling complex that promotes growth cone expansion. J. Neurosci. *25*, 3132-3141.

17. Garvalov, B.K., Flynn, K.C., Neukirchen, D., Meyn, L., Teusch, N., Wu, X., Brakebusch, C., Bamburg, J.R., and Bradke, F. (2007). Cdc42 regulates cofilin during the establishment of neuronal polarity. J. Neurosci. *27*, 13117-13129.

18. Moore, S.W., Biais, N., and Sheetz, M.P. (2009). Traction on immobilized netrin-1 is sufficient to reorient axons. Science *325*, 166.

19. Wang, Y.L., and Pelham, R.J., Jr. (1998). Preparation of a flexible, porous polyacrylamide substrate for mechanical studies of cultured cells. Methods Enzymol. *298*, 489-496.

20. Manser, E., Leung, T., Salihuddin, H., Zhao, Z.S., and Lim, L. (1994). A brain serine/threonine protein kinase activated by Cdc42 and Rac1. Nature *367*, 40-46.

21. Toriyama, M., Shimada, T., Kim, K.B., Mitsuba, M., Nomura, E., Katsuta, K., Sakumura, Y., Roepstorff, P., and Inagaki, N. (2006). Shootin1: A protein involved in the organization of an asymmetric signal for neuronal polarization. J. Cell Biol. *175*, 147-157.

22. Jacobs, T., Causeret, F., Nishimura, Y.V., Terao, M., Norman, A., Hoshino, M., and Nikolic, M. (2007). Localized activation of p21-activated kinase controls neuronal polarity and morphology. J. Neurosci. *27*, 8604-8615.

23. Delorme-Walker, V.D., Peterson, J.R., Chernoff, J., Waterman, C.M., Danuser, G., DerMardirossian, C., and Bokoch, G.M. (2011). Pak1 regulates focal adhesion strength, myosin IIA distribution, and actin dynamics to optimize cell migration. J. Cell Biol. *193*, 1289-1303.

24. Watanabe, N., and Mitchison, T.J. (2002). Single-molecule speckle analysis of actin filament turnover in lamellipodia. Science *295*, 1083-1086.

25. Murray, A., Naeem, A., Barnes, S.H., Drescher, U., and Guthrie, S. (2010). Slit and Netrin-1 guide cranial motor axon pathfinding via Rho-kinase, myosin light chain kinase and myosin II. Neural. Dev. *5*, 16.

26. Bokoch, G.M. (2003). Biology of the p21-activated kinases. Annu. Rev. Biochem. *72*, 743-781.

27. Schmidt, A., and Hall, A. (2002). Guanine nucleotide exchange factors for Rho GTPases: turning on the switch. Genes Dev. *16*, 1587-1609.

28. Kaibuchi, K., Kuroda, S., and Amano, M. (1999). Regulation of the cytoskeleton and cell adhesion by the Rho family GTPases in mammalian cells. Annu. Rev. Biochem. *68*, 459-486.

29. Rohatgi, R., Ma, L., Miki, H., Lopez, M., Kirchhausen, T., Takenawa, T., and Kirschner, M.W. (1999). The interaction between N-WASP and the Arp2/3 complex links Cdc42-dependent signals to actin assembly. Cell *97*, 221-231.

30. Miki, H., Yamaguchi, H., Suetsugu, S., and Takenawa, T. (2000). IRSp53 is an essential intermediate between Rac and WAVE in the regulation of membrane ruffling. Nature *408*, 732-735.

31. Peng, J., Wallar, B.J., Flanders, A., Swiatek, P.J., and Alberts, A.S. (2003). Disruption of the Diaphanous-related formin Drf1 gene encoding mDia1 reveals a role for Drf3 as an effector for Cdc42. Curr. Biol. *13*, 534-545.

32. Huber, A.B., Kolodkin, A.L., Ginty, D.D., and Cloutier, J.F. (2003). Signaling at the growth cone: ligand-receptor complexes and the control of axon growth and guidance. Annu. Rev. Neurosci. *26*, 509-563.

33. Round, J., and Stein, E. (2007). Netrin signaling leading to directed growth cone steering. Curr. Opin. Neurobiol. *17*, 15-21.

34. Guilluy, C., Garcia-Mata, R., and Burridge, K. (2011). Rho protein crosstalk: another social network? Trends Cell Biol. *21*, 718-726.

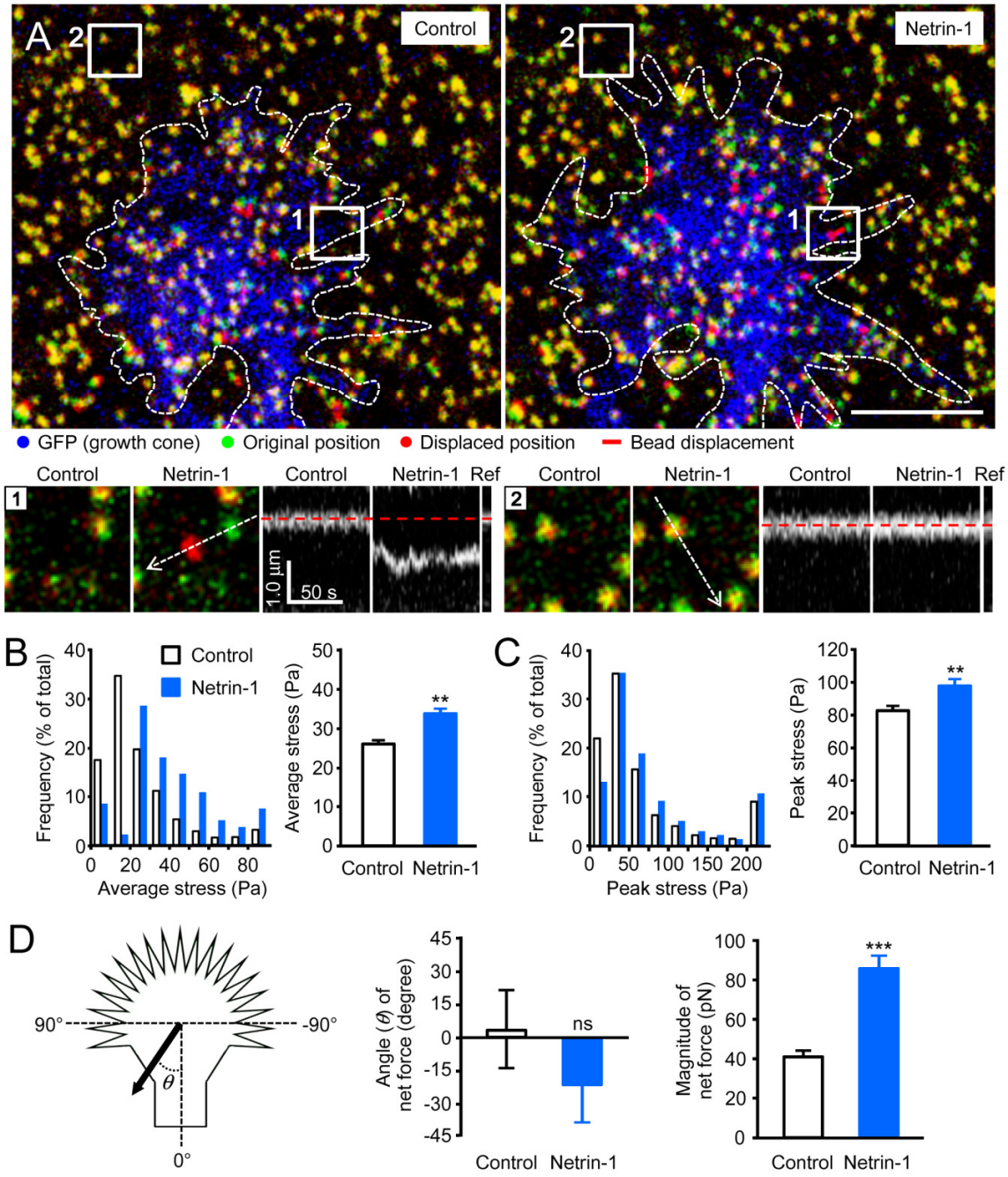
A
Control
Netrin-1
GFP (growth cone)
Original position
Displaced position
Bead displacement
Control
Netrin-1
Ref
1.0 µm
50 s
B
Frequency (% of total)
Average stress (Pa)
C
Peak stress (Pa)
D
90°
-90°
0°
θ
Angle (θ) of net force (degree)
ns
Magnitude of net force (pN)
**
***

Figure 1. Netrin-1 positively regulates traction forces at growth cones

(A) Fluorescent images (upper panel) showing an axonal growth cone of a DIV2 neuron expressing GFP and cultured on L1-CAM-coated polyacrylamide gel embedded with 200-nm fluorescent beads. The pictures show representative images from time-lapse series taken every 2.5 sec for 125 sec before (control) and 60 min after netrin-1 (300 ng/ml) stimulation (see Movie S1). The original and displaced positions of the beads in the gel are indicated by green and red colors, respectively. The bead displacements are also indicated by red bars. Dashed lines indicate the boundary of the growth cone. The kymographs (lower panel) along the axis of bead displacement (white dashed arrows) at the indicated areas 1 and 2 of the growth cone show movement of beads recorded every 2.5 sec. The original positions of the beads determined after the experiment (Ref) are indicated by red dashed lines. The bead in area 2 is a reference bead.

(B and C) Histogram (left) and statistical analyses (right) of the average stress (B) and peak stress (C) under growth cones before or after 60-min netrin-1 stimulation.

(D) Angle (θ) and magnitude of the net force under axonal growth cones before or after netrin-1 stimulation.

Data in (B - D) represent means ± SEM; ***, $P < 0.01$; **, $P < 0.02$; ns, non-significant.

A totally 12 growth cones were examined. Bar: in (A) 5 μm.

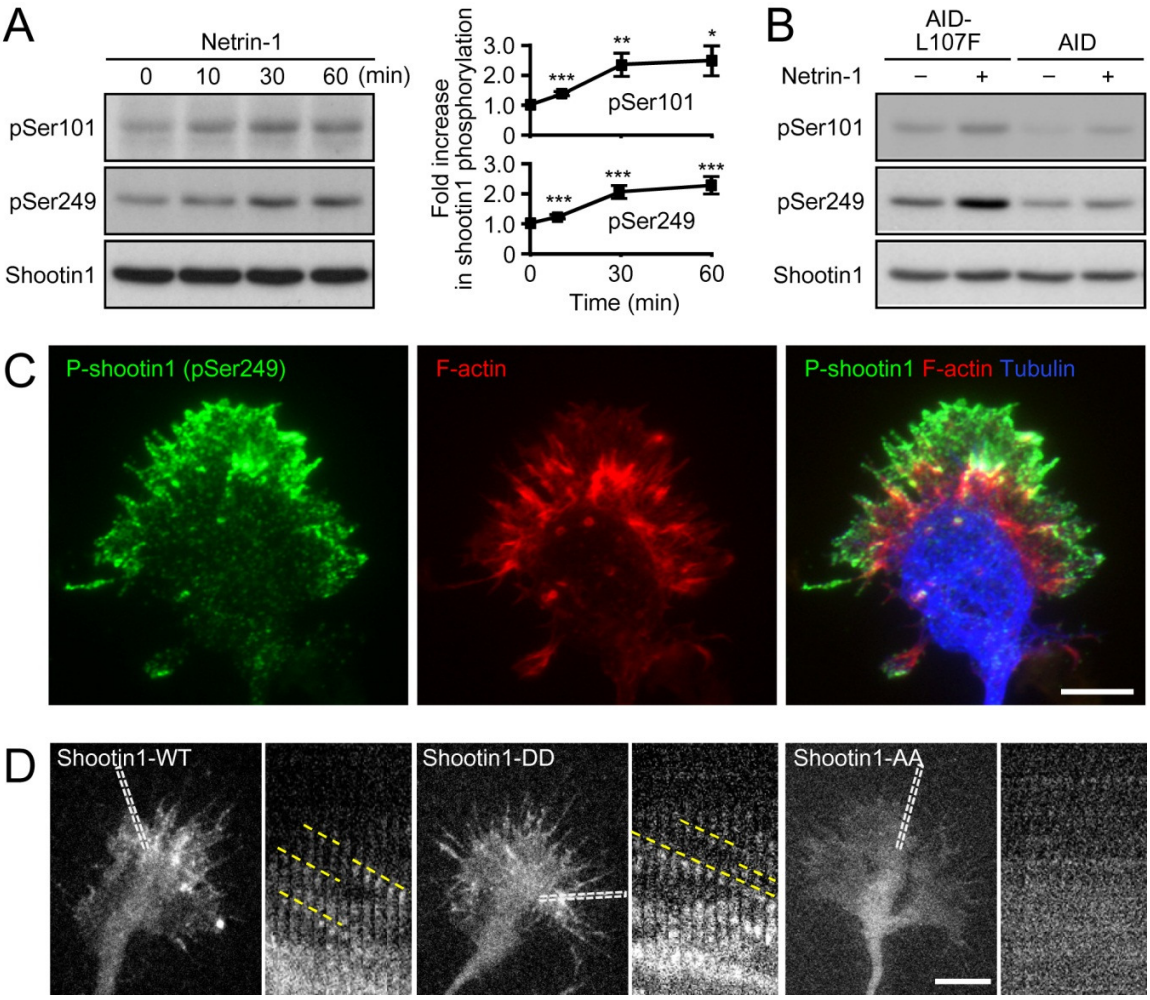
A
Netrin-1
0 10 30 60 (min)
pSer101
pSer249
Shootin1
Fold increase in shootin1 phosphorylation
3.0
2.0
1.0
0
***
**
*
pSer101
***
***
***
pSer249
0 30 60
Time (min)
B
AID-L107F
AID
Netrin-1
– + – +
pSer101
pSer249
Shootin1
C
P-shootin1 (pSer249)
F-actin
P-shootin1 F-actin Tubulin
D
Shootin1-WT
Shootin1-DD
Shootin1-AA

Figure 2. Netrin-1 induces Pak1-mediated shootin1 phosphorylation, which in turn enhances the interaction between shootin1 and F-actin retrograde flow at axonal growth cones

(A) DIV2 neurons were treated with 300 ng/ml netrin-1. Cell lysates were then analyzed by immunoblot with anti-pSer101-shootin1, anti-pSer249-shootin1 and anti-shootin1 antibodies.

(B) Neurons expressing AID-L107F (control) or AID (DN-Pak1) were treated with netrin-1 for 60 min, and examined by immunoblot.

(C) Fluorescence images of an axonal growth cone co-stained with anti-pSer249-shootin1 antibody (green), Alexa-594 phalloidin (red), and anti-β3-tubulin antibody (blue).

(D) Fluorescent speckle images of EGFP-shootin1-WT, EGFP-shootin1-DD, and EGFP-shootin1-AA in axonal growth cones (see Movies S2). Kymographs of the indicated rectangular regions at 5-sec intervals are shown to the right (flows of shootin1 speckles are indicated by dashed yellow lines).

Data in (A) represent means ± SEM; ***, $p < 0.01$; **, $p < 0.02$; *, $p < 0.05$. Scale bars in (C and D) represent 5 mm.

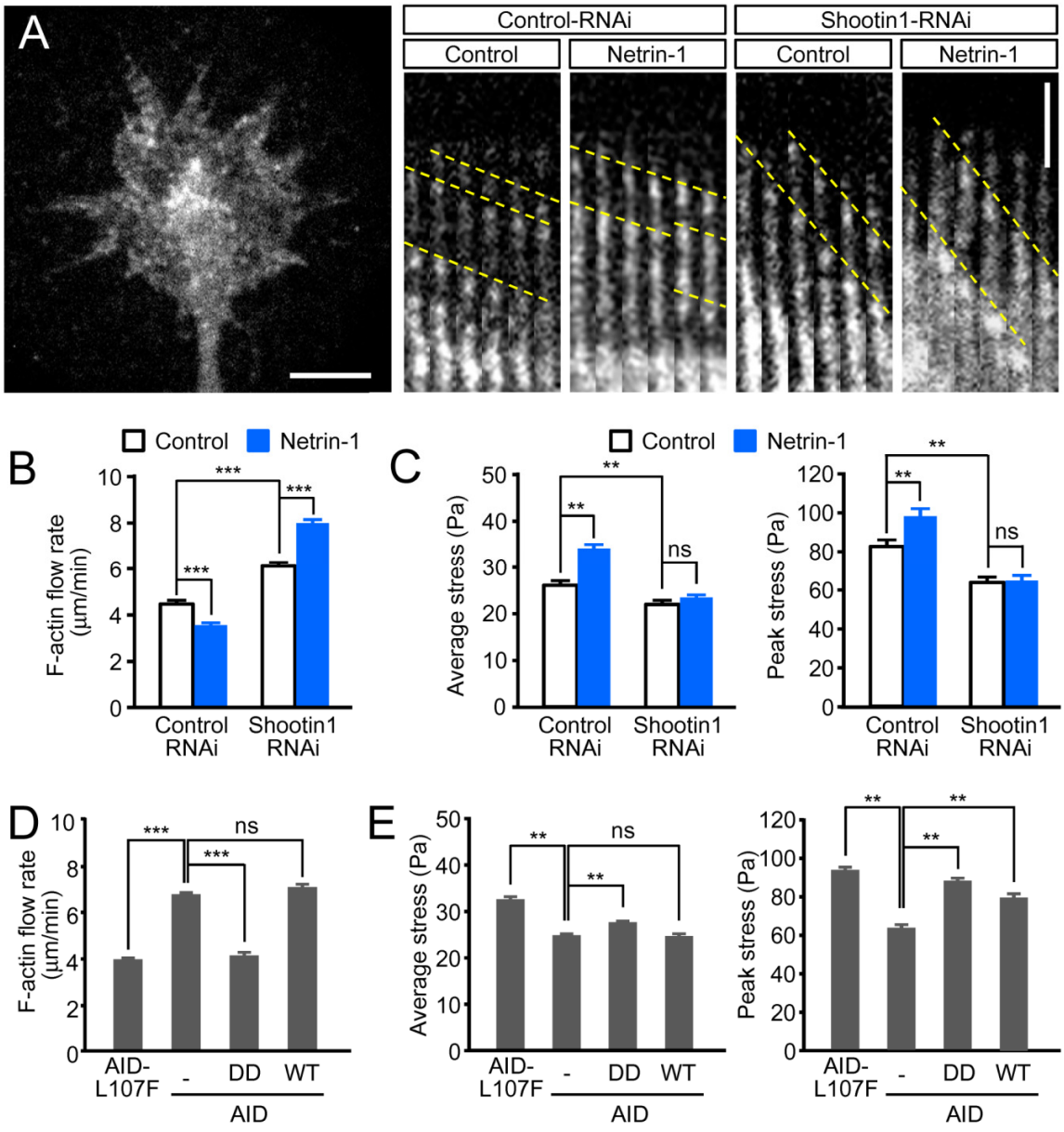
A
Control-RNAi
Shootin1-RNAi
Control
Netrin-1
Control
Netrin-1
B
Control
Netrin-1
F-actin flow rate (μm/min)
Control RNAi
Shootin1 RNAi
C
Average stress (Pa)
Peak stress (Pa)
ns
D
E
AID-L107F
-
DD
WT
AID

Figure 3. Pak1-mediated shootin1 phosphorylation promotes clutch engagement and transmission of traction forces at axonal growth cones

(A) Fluorescent speckle images of mRFP-actin at axonal growth cones expressing control miRNA (see Movie S3) or miRNA against shootin1 (shootin1 RNAi) in the presence or absence of 300 ng/ml netrin-1. Kymographs of mRFP-actin speckles in filopodia at 5-sec intervals are shown to the right (F-actin flows are indicated by dashed yellow lines).

(B) F-actin retrograde flow rate in filopodia and lamellipodia measured by kymograph analysis in (A) (671 speckles were examined).

(C) Neurons expressing control miRNA or shootin1 miRNA were cultured on polyacrylamide gels containing 200-nm fluorescent beads in the presence or absence of 300 ng/ml netrin-1 for 60 min. Average stress and peak stress were calculated from displacement of beads under the growth cones (26 growth cones were examined).

(D) F-actin retrograde flow rate in filopodia and lamellipodia measured in neurons co-expressing AID-L107F (control) or AID (DN-Pak1) with shootin1-WT or shootin1-DD (686 speckles were examined).

(E) Neurons co-expressing AID-L107F or AID with shootin1-WT or shootin1-DD were cultured on polyacrylamide gels containing fluorescent beads, and average stress and peak stress were measured (65 growth cones were examined).

Data in (B-E) represent means ± SEM; ***, $P < 0.01$; **, $P < 0.02$; ns, non-significant. Bars: 5 μm.

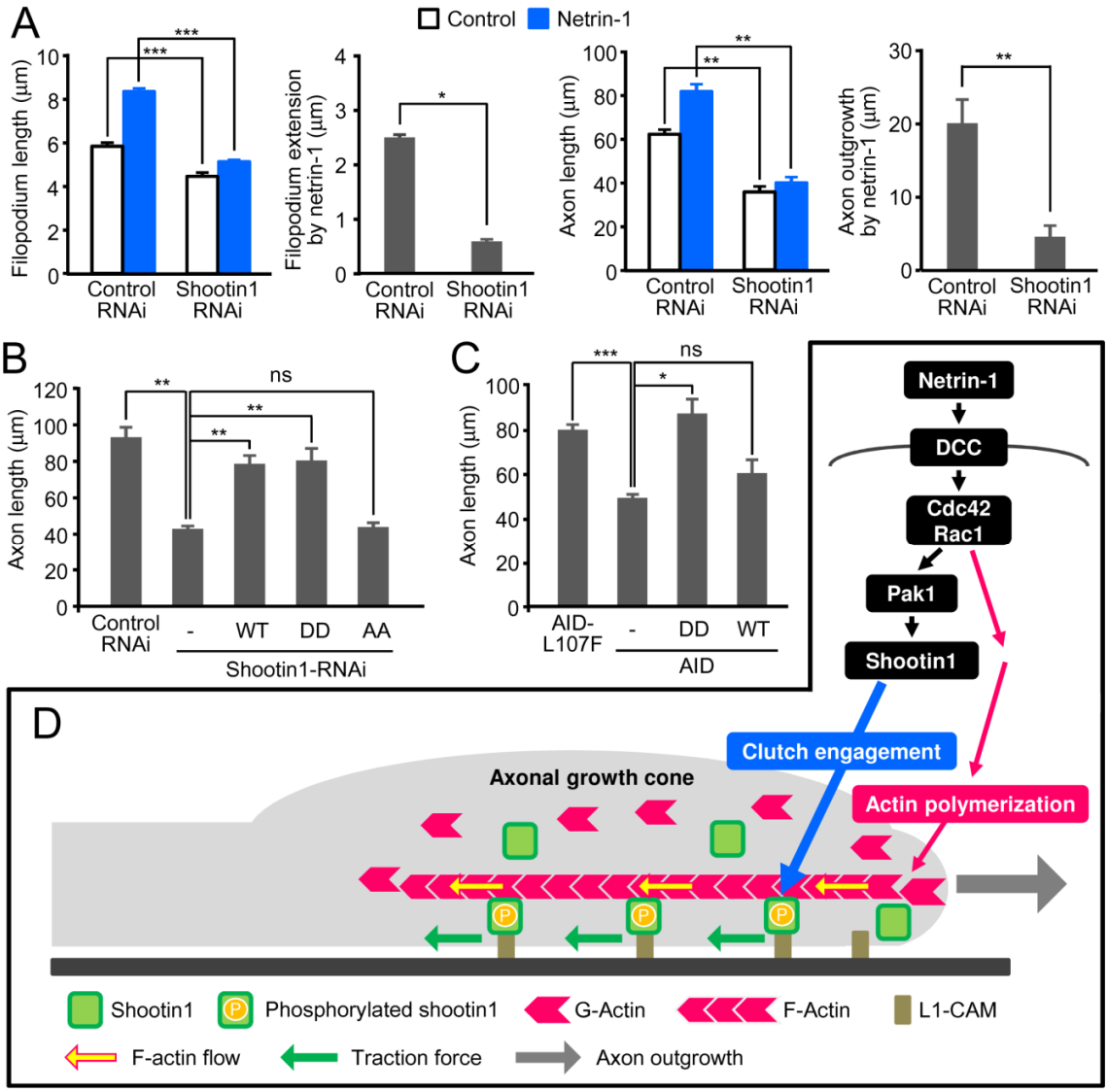
A
Control
Netrin-1
Filopodium length (μm)
Control RNAi
Shootin1 RNAi
Filopodium extension by netrin-1 (μm)
Axon length (μm)
Axon outgrowth by netrin-1 (μm)
B
Axon length (μm)
Control RNAi
-
WT
DD
AA
Shootin1-RNAi
ns
C
Axon length (μm)
AID-L107F
-
DD
WT
AID
ns
Netrin-1
DCC
Cdc42
Rac1
Pak1
Shootin1
D
Axonal growth cone
Clutch engagement
Actin polymerization
Shootin1
Phosphorylated shootin1
G-Actin
F-Actin
L1-CAM
F-actin flow
Traction force
Axon outgrowth

Figure 4. Pak1-mediated shootin1 phosphorylation promotes filopodium extension and axon outgrowth

(A) Neurons expressing control miRNA or shootin1 miRNA were incubated with BSA (control) or 300 ng/ml netrin-1 for 60 min or 24 h. Filopodium length at axonal growth cones (after 60 min) and axon length (after 24 h) were then analyzed (n = 3, 976 filopodia and 908 axons were examined). The neuronal morphology was analyzed at DIV2.

(B and C) Neurons co-expressing control miRNA or shootin1 miRNA with an RNAi-refractory mutant of shootin1 (WT, DD, or AA) (B), or co-expressing AID-L107F (control) or AID (DN-Pak1) with shootin1-WT or shootin1-DD (C), were cultured for 24 h. Axon length was then analyzed (n = 3, 908 axons were examined for (B) and 1893 axons were examined for (C)).

Data in (A-C) represent means ± SEM; ***, $P < 0.01$; **, $P < 0.02$; *, $P < 0.05$; ns, non-significant.

(D) A model for signal–force conversion for axon outgrowth. Netrin-1, via activation of DCC (netrin-1 receptor), Cdc42 and Rac1, induces Pak1-mediated shootin1 phosphorylation (black arrows), thereby enhancing clutch engagement through shootin1-F-actin interaction (blue arrow). Clutch engagement converts the F-actin flow (yellow arrows) into traction forces exerted on the substrate (green arrows). This engagement also reduces the speed of the F-actin flow, converting actin polymerization into protrusion of the leading edge (gray arrow). Clutch engagement (blue arrow) and Cdc42- and Rac1-induced actin polymerization (red arrows) may work coordinately to effectively regulate mechanical forces for cell motility.

Supplemental Information

Conversion of a Signal into Forces for Axon Outgrowth through Pak1-mediated Shootin1 Phosphorylation

Michinori Toriyama, Satoshi Kozawa, Yuichi Sakumura and Naoyuki Inagaki

Supplemental Inventory

Supplemental Results

A recent study reported that shootin1 associates with profilin IIa [35], thereby raising the possibility that shootin1 might affect F-actin flow by directly regulating actin assembly. However, knockdown of endogenous shootin1 in hippocampal neurons did not alter F-actin content in the growth cones (Figure S3B). Therefore, it appears that shootin1 does not affect actin polymerization.

This conclusion is further supported by our fluorescent speckle microscopy data. Shootin1 RNAi led to a significant increase in the F-actin flow rate in the growth cones (data suggesting the slippage of the clutch engagement; Figure 3A and B). If shootin1 could promote traction force and axon outgrowth by activating actin assembly, it would be involved in the promotion of F-actin flow. In this case, shootin1 RNAi would lead to a decrease in the F-actin flow rate. However, the inverse effect was observed. Thus, we consider that shootin1 promotes traction force and axon outgrowth by increasing clutch engagement, not by increasing actin assembly thorough profilin IIa.

Supplemental Discussion

Figure S3A describes a mechanical explanation for the effects of netrin-1 stimulation and shootin1 RNAi on F-actin retrograde flow, traction force, and axon outgrowth. In control neurons (upper panel), netrin-1 stimulation, through activation of Cdc42 and Rac1 and Pak1-mediated shootin1 phosphorylation (black arrows), promotes clutch engagement (blue arrow), thereby converting the F-actin retrograde flow into traction forces exerted on the substrate (green arrows). This engagement also reduces the speed of the F-actin retrograde flow (yellow arrow) and converts actin polymerization into axon outgrowth (grey arrow). Activation of Cdc42 and Rac1 would stimulate actin polymerization at the leading edge (red arrows); however, the enhancement of actin polymerization would not be significant because increased counter-force at the leading edge membrane (brown arrow) would mechanically inhibit actin polymerization, as suggested previously [36, 37].

A decrease in shootin1 level by RNAi (lower panel) reduces basal clutch engagement, resulting in increased slippage between F-actin and L1-CAM and an increased velocity of F-actin retrograde flow (yellow arrow). Clutch disengagement also reduces counter-force at the leading edge membrane, thereby accelerating actin polymerization at the leading edge [36, 37]. With decreased counter-force at the leading edge (brown arrow), netrin-1 stimulation, via activation of Cdc42 and Rac1, enhances significantly actin

polymerization at the leading edge (red arrows). The push from actin polymerization further accelerates actin retrograde flow (yellow arrow).

Figure S3C shows the rate of actin polymerization determined from the data in Figures 3A and 3B, as the sum of F-actin extension and retrograde flow at the leading edge [38]. These data and the results in Figure 3B are consistent with the present explanation.

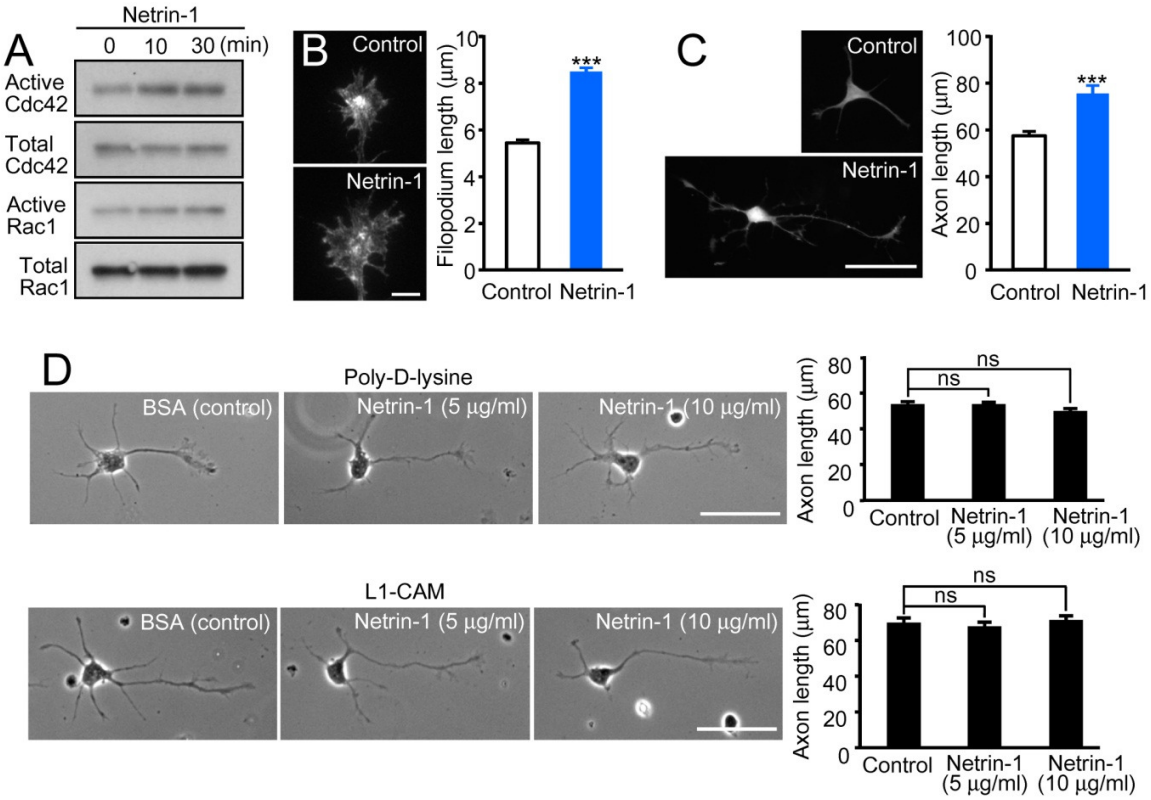
A
Netrin-1
0 10 30 (min)
Active Cdc42
Total Cdc42
Active Rac1
Total Rac1
B
Control
Netrin-1
Filopodium length (μm)
***
Control Netrin-1
C
Control
Netrin-1
Axon length (μm)
***
Control Netrin-1
D
Poly-D-lysine
BSA (control)
Netrin-1 (5 μg/ml)
Netrin-1 (10 μg/ml)
Axon length (μm)
ns
Control
Netrin-1 (5 μg/ml)
Netrin-1 (10 μg/ml)
L1-CAM
BSA (control)
Netrin-1 (5 μg/ml)
Netrin-1 (10 μg/ml)
Axon length (μm)
ns
Control
Netrin-1 (5 μg/ml)
Netrin-1 (10 μg/ml)
E
Actin
Original position
Displaced position
Actin
Beads
Ref
1
2
3
2 μm
1 min

Figure S1.

(A-D) Netrin-1 positively regulates filopodium extension and axon outgrowth.

(**A**) DIV2 neurons were treated with 300 ng/ml netrin-1 for the indicated periods. Cdc42 and Rac1 activities were then analyzed by pull-down assay. Active Cdc42 and Rac1, bound to GST-Pak1-CRIB, and total cell lysate were analyzed by immunoblot with anti-Cdc42 and anti-Rac1 antibodies. (**B**) Fluorescence images of axonal growth cones of DIV2 neurons incubated with BSA (control) or 300 ng/ml netrin-1 for 60 min and stained with Alexa-594 phalloidin. The graph to the right shows the lengths of growth cone filopodia (546 filopodia were examined). (**C**) Fluorescence images of EGFP-expressing neurons cultured in the presence of BSA (control) or 300 ng/ml netrin-1 for 24 h. The graph to the right shows axon lengths (539 axons were examined). **(D)** Neurons were cultured on coverslips coated without L1-CAM (poly-D-lysine) (upper panel) or with L1-CAM (lower panel) onto which netrin-1 (5 or 10 μg/ml) or BSA (control) was pre-absorbed. Axon length was then measured. DIV2 neurons (upper panel) on poly-D-lysine with or without netrin-1 pre-absorption (for 3 h) were fixed and analyzed (a total of 697 cells were examined). DIV1 neurons (lower panel) on L1-CAM with or without netrin-1 pre-absorption (for 3 h) were fixed and analyzed (a total of 1589 cells were examined). The graph to the right shows axon lengths.

(E) The relationship between F-actin retrograde flow and bead displacement.

Fluorescence micrographs (upper panel) showing an axonal growth cone of a DIV2 hippocampal neuron expressing EGFP-actin (right) and cultured on L1-CAM-coated polyacrylamide gel embedded with 200-nm fluorescent beads (left). The original and displaced positions of the beads in the gel are indicated by green and red colors, respectively. Dashed lines indicate the boundary of the growth cone. Kymographs (lower panel) along the arrows 1-3 show the retrograde movements of EGFP-actin and bead displacement at the growth cone (recorded every 5.0 sec for 125 sec). The borders of the cellular leading edge are indicated by the blue arrow. Fluorescent beads under and outside the growth cone are indicated by red and black arrowheads, respectively. The original positions of the beads (Ref) are shown at the right of each panel.

Data represent means ± SEM; ***, $P < 0.01$; ns, non-significant. Bars: in (**B** and **E**) 5 μm; in (**C** and **D**) 50 μm.

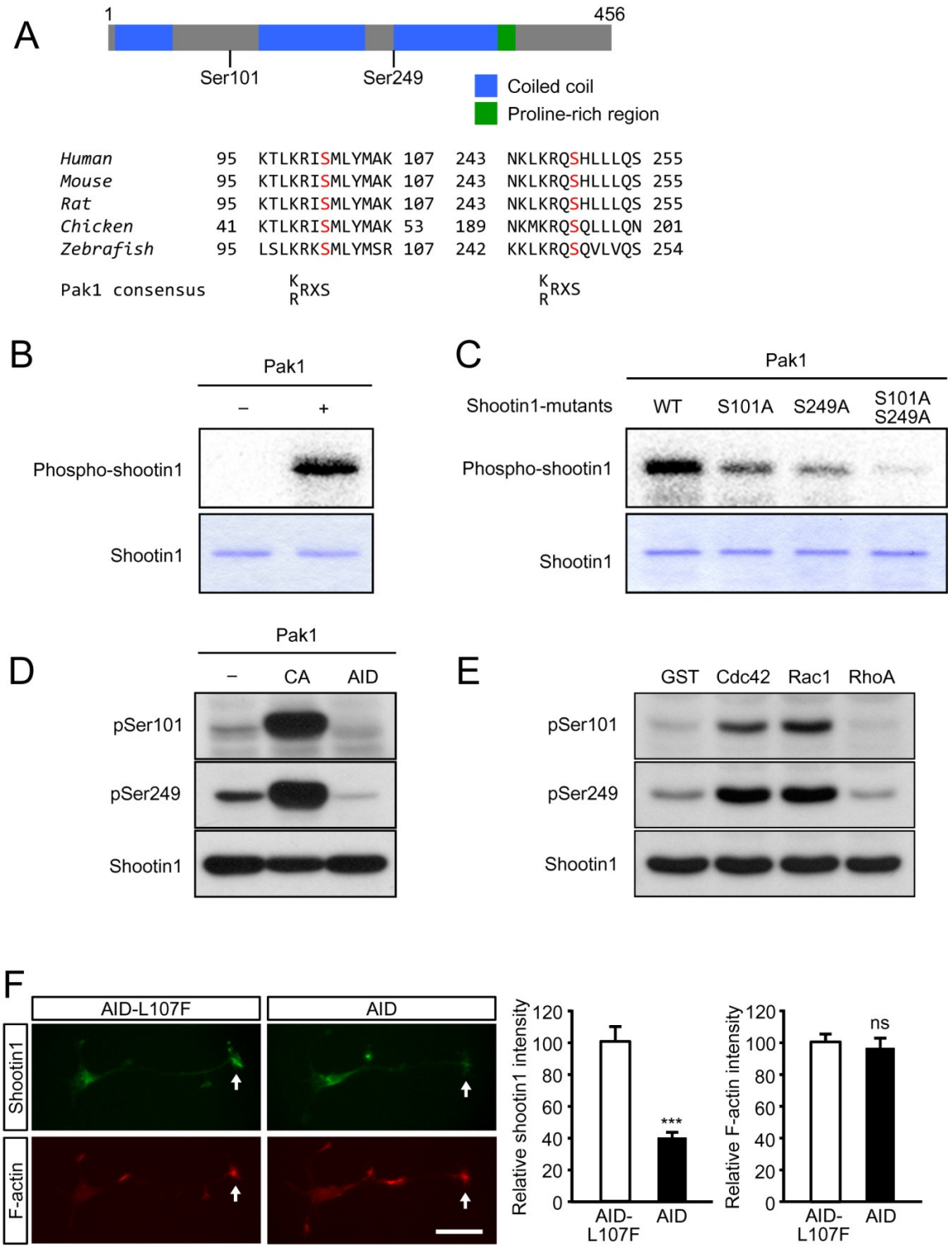
A
1
456
Ser101
Ser249
Coiled coil
Proline-rich region
Human 95 KTLKRISMLYMAK 107 243 NKLKRQSHLLLQS 255
Mouse 95 KTLKRISMLYMAK 107 243 NKLKRQSHLLLQS 255
Rat 95 KTLKRISMLYMAK 107 243 NKLKRQSHLLLQS 255
Chicken 41 KTLKRISMLYMAK 53 189 NKMKRQSQLLLQN 201
Zebrafish 95 LSLKRKSMLYMSR 107 242 KKLKRQSQVLVQS 254
Pak1 consensus K/R RXS K/R RXS
B
Pak1
–
+
Phospho-shootin1
Shootin1
C
Pak1
Shootin1-mutants
WT
S101A
S249A
S101A S249A
Phospho-shootin1
Shootin1
D
Pak1
–
CA
AID
pSer101
pSer249
Shootin1
E
GST
Cdc42
Rac1
RhoA
pSer101
pSer249
Shootin1
F
AID-L107F
AID
Shootin1
F-actin
Relative shootin1 intensity
120
100
80
60
40
20
0
***
AID-L107F
AID
Relative F-actin intensity
120
100
80
60
40
20
0
ns
AID-L107F
AID

Figure S2.

(A-E) Pak1 phosphorylates shootin1 at Ser101 and Ser249 *in vitro* and in neurons.

(**A**) Identified phosphorylation sites of shootin1 and comparison of sequences flanking each phosphorylation site among several species. A consensus phosphorylation sequence for Pak1 is shown below. (**B** and **C**) *In vitro* kinase assays were performed using purified wild type (WT) or unphosphorylated mutants (S101A, S249A, or S101A/S249A) of shootin1. After a 30-min reaction with Pak1, protein mixtures were subjected to SDS-PAGE and visualized by autoradiography and Coomassie Brilliant Blue staining. (**D** and **E**) Cell lysates from DIV2 cultured neurons were analyzed by immunoblotting with anti-pSer101-shootin1, anti-pSer249-shootin1, and anti-shootin1 antibodies. Neurons were transfected with constitutively active Pak1 (CA-Pak1) or dominant negative Pak1 (AID) (**D**), or with constitutively active Cdc42, constitutively active Rac1, constitutively active RhoA, or GST (control) (**E**).

(F) Pak1-mediated shootin1 phosphorylation enhances the interaction between shootin1 and F-actin at axonal growth cones.

Neurons were transfected with AID-L107F (control) or AID (DN-Pak1), and co-stained with anti-shootin1 antibody and Alexa-594 phalloidin. The relative fluorescence intensities of shootin1 and F-actin at axonal growth cones (arrows) were measured (right) (n = 69 cells for AID-L107F and 63 cells for AID were examined).

Data represent means ± SEM; ***, $P < 0.01$; ns, non-significant. Bar: in (**F**) 20 μm.

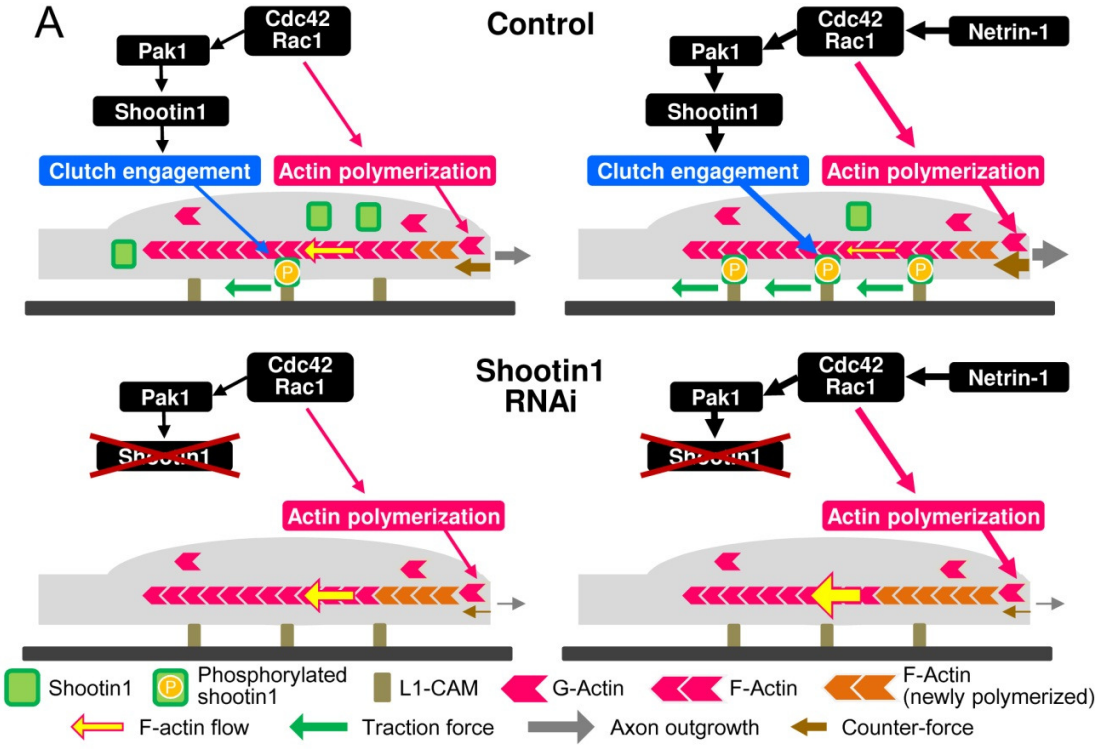
A
Control
Pak1
Cdc42
Rac1
Shootin1
Clutch engagement
Actin polymerization
Netrin-1
Shootin1
RNAi
Shootin1
Phosphorylated shootin1
L1-CAM
G-Actin
F-Actin
F-Actin (newly polymerized)
F-actin flow
Traction force
Axon outgrowth
Counter-force

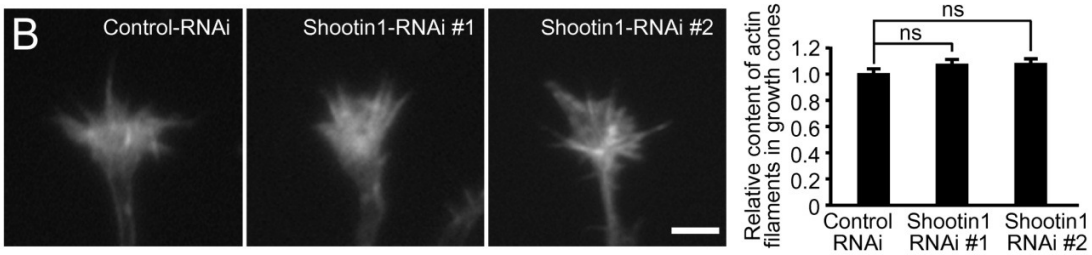
B
Control-RNAi
Shootin1-RNAi #1
Shootin1-RNAi #2
Relative content of actin filaments in growth cones
ns
ns
Control RNAi
Shootin1 RNAi #1
Shootin1 RNAi #2

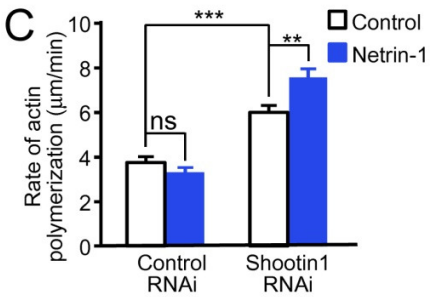
C
Rate of actin polymerization (μm/min)
***
**
ns
Control
Netrin-1
Control RNAi
Shootin1 RNAi

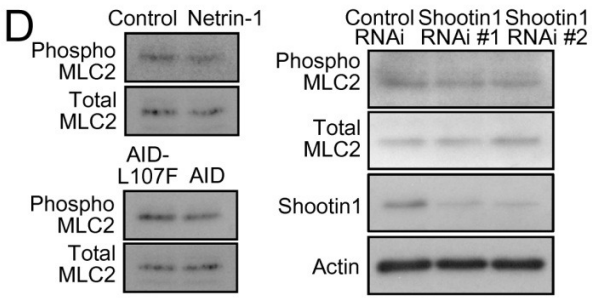
D
Control Netrin-1
Phospho MLC2
Total MLC2
AID-L107F AID
Control RNAi
Shootin1 RNAi #1
Shootin1 RNAi #2
Shootin1
Actin

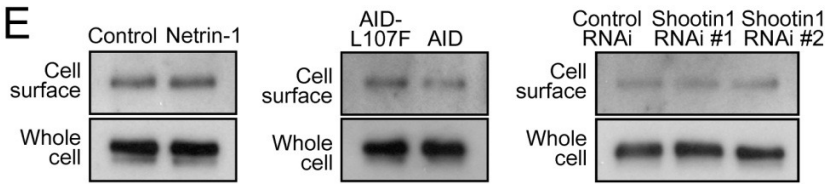
E
Control Netrin-1
AID-L107F AID
Control RNAi
Shootin1 RNAi #1
Shootin1 RNAi #2
Cell surface
Whole cell

Figure S3.

(A and C) A mechanical explanation for the effects of netrin-1 stimulation and shootin1 RNAi on F-actin retrograde flow, traction force, and axon outgrowth.

For details, see Supplemental Discussion. (**C**) The rate of actin polymerization determined from the kymograph analysis data in Figures 3A and 3B, as the sum of F-actin extension and retrograde flow at the leading edge [38].

(B) Effects of shootin1 RNAi on F-actin content in growth cones.

Neurons were transfected with control-miRNA or shootin1-miRNA vectors, and stained with Alexa-594 phalloidin at DIV2. The graph to the right shows the fluorescence intensity of F-actin in the growth cones (a total of 503 neurons were examined).

(D) Effects of netrin-1 stimulation, Pak1 inhibition or shootin1 RNAi on Myosin II activity in cultured neurons.

Myosin II activity was analyzed by monitoring the phosphorylation of the regulatory light chain of myosin II (myosin light chain 2, MLC2) at Ser19. Neurons on DIV2 were analyzed by immunoblot with anti-phospho-MLC2 antibody, anti-MLC2 antibody, anti-shootin1 antibody or anti-actin antibody. Upper left panel: neurons were treated with 300 ng/ml netrin-1 or BSA (control) for 60 min. Lower left panel: neurons were transfected with AID-L107F (control) or AID (DN-Pak1). Right panel: neurons were transfected with control miRNA or shootin1 miRNA.

(E) Effects of netrin-1 stimulation, Pak1 inhibition or shootin1 RNAi on L1-CAM expression on the neuronal cell surface.

Cell surface expression of L1-CAM in cultured neurons at DIV2 was evaluated by biotinylation assay. Biotinylated L1-CAM molecules on the cell surface were isolated with streptavidin-agarose beads and visualized by immunoblot using anti-L1-CAM antibody. Left panel: neurons were treated with 300 ng/ml netrin-1 for 60 min (n = 6). Center panel: neurons were transfected with AID-L107F (control) or AID (DN-Pak1) (n = 3). Right panel: neurons expressing control miRNA or shootin1 miRNA (n = 3). Statistical analyses of the relative band intensities showed non-significant difference (data not shown).

Data represent means ± SEM; ***, $P < 0.01$; **, $P < 0.02$; ns, non-significant. Bar: in (**B**) 5 μm.

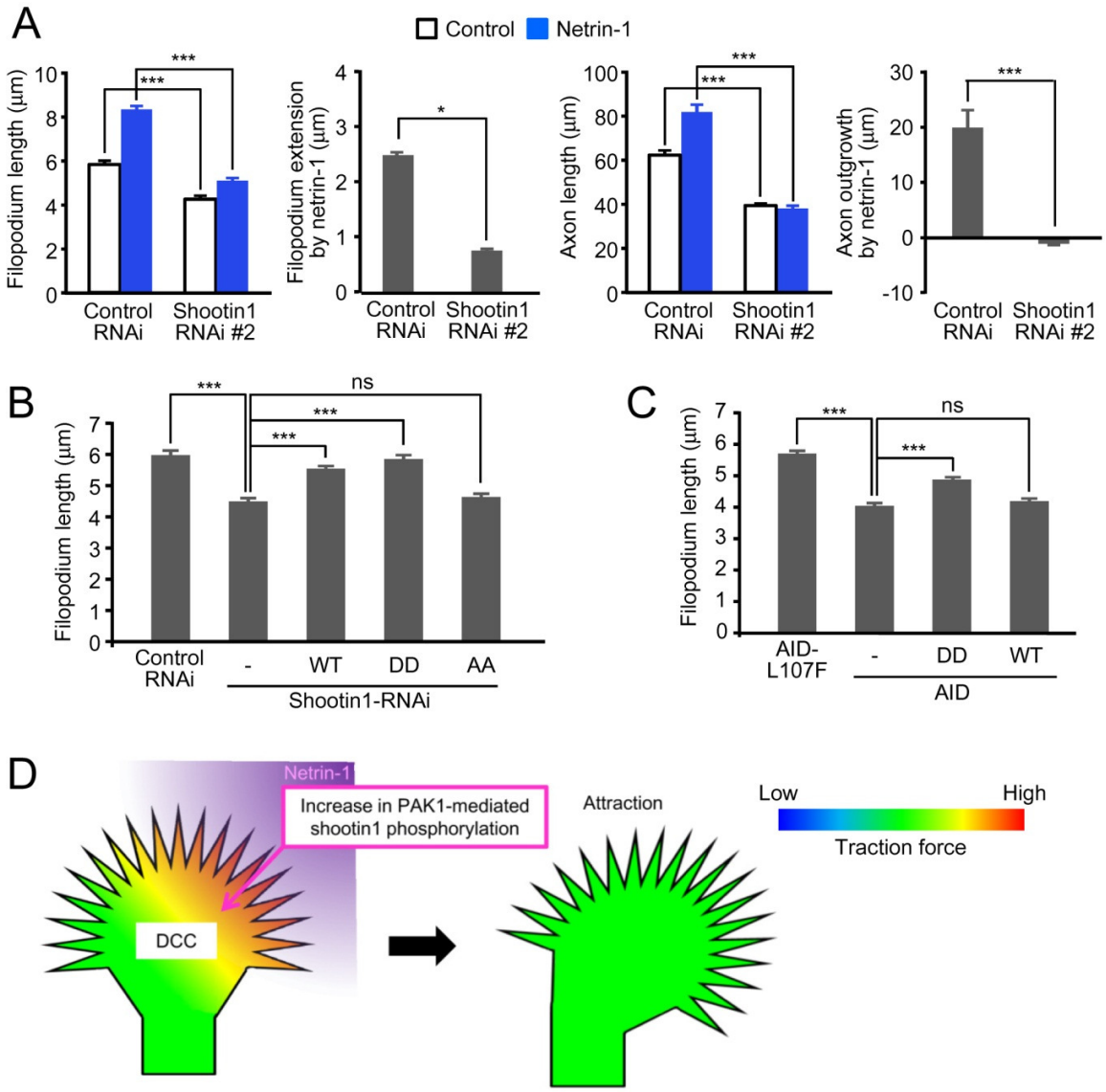
A
Control
Netrin-1
Filopodium length (μm)
Control RNAi
Shootin1 RNAi #2
Filopodium extension by netrin-1 (μm)
Axon length (μm)
Axon outgrowth by netrin-1 (μm)
B
Filopodium length (μm)
Control RNAi
-
WT
DD
AA
Shootin1-RNAi
ns
C
Filopodium length (μm)
AID-L107F
-
DD
WT
AID
ns
D
Netrin-1
Increase in PAK1-mediated shootin1 phosphorylation
DCC
Attraction
Low
High
Traction force

Figure S4.

(A) Effects of shootin1 miRNA #2, an alternative shootin1 miRNA, on netrin-1-induced filopodium extension and axon outgrowth.

The targeting sequence of shootin1 miRNA #2 is distinct from that of shootin1 miRNA used in Figure 4A. Neurons expressing control miRNA or shootin1 miRNA were incubated with BSA (control) or 300 ng/ml netrin-1 for 60 min or 24 h. Filopodium length at axonal growth cones (after 60 min) and axon length (after 24 h) were then analyzed (907 filopodia and 919 axons were examined). The neuronal morphology was analyzed at DIV2.

(B and C) Pak1-mediated shootin1 phosphorylation promotes filopodium extension.

Neurons co-expressing control miRNA or shootin1 miRNA with an RNAi-refractory mutant of shootin1 (WT, DD, or AA) (**B**), or co-expressing AID-L107F (control) or AID (DN-Pak1) with shootin1-WT or shootin1-DD (**C**), were cultured for 24 h. Filopodium length at axonal growth cones was then analyzed (n = 3, 1121 filopodia were examined for (**B**) and 1667 filopodia were examined for (**C**)).

(D). A model for netrin-1-mediated axon attraction.

See Results and Discussion for details.

Data represent means ± SEM; ***, $P < 0.01$; *, $P < 0.05$; ns, non-significant.

Supplemental Movies

Movie S1. Netrin-1-induced promotion of traction forces at an axonal growth cone (see Figure 1A). Left and right panels show bead displacement before and 60 min after netrin-1 stimulation, respectively.

Movie S2. Fluorescent speckle dynamics of EGFP-shootin1-WT, EGFP-shootin1-DD and EGFP-shootin1-AA at an axonal growth cone (see Figure 2D).

Movie S3. Fluorescent speckle dynamics of mRFP-actin at an axonal growth cone (see Figure 3A).

Supplemental Experimental Procedures

Cell culture, transfection, and RNAi

Hippocampal neurons prepared from E18 rat embryos were cultured on glass coverslips (Matsunami) coated with L1-CAM-FC as described [11]. All experiments except for the measurement of forces were carried out on L1-CAM-coated glass surfaces. Neurons were transfected with plasmid DNA using Nucleofector (Lonza) before plating. For RNAi experiments, to ensure a high level of expression of miRNA before axon outgrowth, neurons were cultured in suspension on non-coated polystyrene dishes for 24 h [21], and then collected and seeded onto coated-glass coverslips, polyacrylamide gels, or glass bottom dishes. For the immunoblot analyses in Figures 2B, S4D, and S4E, we used cortical neurons, which also respond to Netrin-1 [14], as the experiments required large numbers of neurons. These were prepared from E18 rat embryos using the same protocol as above. For RNAi experiments, we used a Block-iT Pol II miR RNAi expression kit (Invitrogen). The targeting sequence of shootin1 miRNA was reported previously [21]; that of another miRNA (shootin1 RNAi #2), 5'-GTTAGAGGAACGGCTAGAGAA-3', corresponds to nucleotides 867-887 in the coding region of rat shootin1. Reduction of endogenous shootin1 in neurons was confirmed by immunocytochemistry with anti-shootin1 antibody.

DNA constructs

Preparation of the vectors to express wild-type shootin1 has been described previously [21]. RNAi-refractory shootin1 mutants were generated using a QuickChange II site-directed mutagenesis kit (Stratagene) as described [11]. Unphosphorylated (S101A/S249A: AA) or phosphomimic (S101D/S249D: DD) mutants of shootin1 were generated with the same kit, to replace each serine with alanine or aspartate, using the following primers: S101A, 5'-CGTTGAAAAGAATCGCCATGTTGTACATGGCCAAGCTGGGACC-3'; S101D, 5'-CGTTGAAAAGAATCGACATGTTGTACATGGCCAAGCTGGGACC-3'; S249A, 5'-CAAGCTAAAGAGACAAGCCCACCTTCTGCTGCAGAGCTCCATC-3'; and S249D, 5'-CAAGCTAAAGAGACAAGACCACCTTCTGCTGCAGAGCTCCATC-3'. cDNAs were sub-cloned into pGEX-6P-1 (GE Healthcare), pEGFP-C1 (Clontech) and pCMV-myc-3B (Stratagene). Pak1 plasmids were kindly provided by Drs. M. Inagaki and L. Lim. Constitutively active Pak1 (CA-Pak1) was described previously [39]. The autoinhibitory domain (AID; aa 83-149) of Pak1 and its mutant AID-L107F were used as dominant negative Pak1 (DN-Pak1) and control, respectively, as reported previously [40].

Plasmids for constitutively active Cdc42, Rac1, and RhoA [41] were kindly provided by Dr. K. Kaibuchi.

Protein and antibody preparation

Recombinant shootin1 was expressed in *Escherichia coli* as a GST fusion protein and purified on a Glutathione Sepharose column (GE Healthcare), after which GST was removed from shootin1 by PreScission protease (GE Healthcare). L1-CAM-FC was prepared as described [11]. Polyclonal antibodies against shootin1 phosphorylated at Ser101 (anti-pSer101-shootin1 antibody) and Ser249 (anti-pSer249-shootin1 antibody) were raised by immunizing rabbits with the synthetic phosphopeptides TLKRI[pS]MLYMC and KLKRQ[pS]HLLLC, respectively. The antibodies were purified using a phosphopeptide affinity column, and absorbed by non-phosphopeptide affinity column to ensure their specificity [42]. Preparation of anti-shootin1 antibody has been described previously [21]. Netrin-1 and Tuj1 were obtained from R&D Systems and Covance, respectively.

In vitro *kinase assay*

Kinase reactions were carried out in 120 μl kinase buffer (50 mM HEPES (pH 7.5), 10 mM $MgCl_2$, 2 mM $MnCl_2$, 1 mM DTT, 10 μCi [γ-^{32}P]ATP, and 25 μM ATP) containing 50 ng active GST-Pak1 (Invitrogen) and 250 ng purified shootin1-WT or its unphosphorylated mutants. After incubation at 30°C for 30 min, the reactions were stopped by adding 5x SDS sample buffer and boiled. The reaction mixtures were subjected to SDS-PAGE and analyzed using autoradiography and **Coomassie Brilliant Blue** staining.

Immunocytochemistry, immunoblot, and microscopy

Cultured neurons were fixed with 3.7% formaldehyde in Krebs buffer for 10 min at room temperature, followed by treatment for 15 min with 0.05% Triton X-100 in PBS on ice and 10% fetal bovine serum in PBS for 1 h at room temperature. They were then stained with antibodies and Alexa-594 phalloidin (Invitrogen), as described [11]. Immunoblot was performed as described [21].

Fluorescence and phase-contrast images of neurons were acquired using a fluorescence microscope (Axioplan2; Carl Zeiss) equipped with a plan-Neofluar 40x 0.75 NA or 63x oil 1.40 NA objective (Carl Zeiss), a charge-coupled device camera (AxioCam

MRm; Carl Zeiss), and imaging software (Axiovision3; Carl Zeiss). The length of filopodia and axons, and the relative fluorescence intensity of shootin1 or F-actin, were measured using Multi Gauge software (Fujifilm). Fluorescent speckle imaging and speckle tracking analysis were performed as described previously [11].

Rac1 and Cdc42 activity assays

Rac1 and Cdc42 activity assays were performed as described [43]. Cells were lysed with GSH-FISH buffer (50 mM Tris-HCl (pH 7.5), 100 mM NaCl, 2 mM $MgCl_2$, 10% glycerol, 1% NP-40, 2 mM phenylmethylsulfonyl fluoride, and 2 μg/ml leupeptin) and centrifuged for 15 min at 17,400 *g* at 4°C. The supernatants were incubated with 2 μg of GST-Pak1-CRIB protein bound to Glutathione Sepharose 4B for 90 min at 4°C. The beads were washed three times with GSH-FISH buffer and bound proteins were eluted in 1x SDS sample buffer. Bound Rac1 and Cdc42 were analyzed by immunoblot using anti-Rac1 (Upstate Group) or anti-Cdc42 (BD Transduction Laboratories) antibodies.

Traction force microscopy

Polyacrylamide gel substrates were prepared as reported [12, 19, 44], with slight modifications. Briefly, glass bottom dishes (No. 0, Matsunami) were treated with 0.1 N NaOH for 15 min and incubated with 2% (v/v) 3-aminopropyltrimethyoxysilane (Sigma) in 2-propanol for 15 min. After washing with H_2O, 0.5 % glutaraldehyde (Sigma) solution was dropped onto the glass and incubated for 30 min. The glass bottom dishes were then washed with H_2O and dried before use. The acrylamide and Bis-acrylamide stock solutions (Nacalai tesque) were diluted to 3.75% and 0.03%, respectively, as reported [44]. Five hundred μl of solution was degassed for 30 min, and then 50 μl of fluorescent microspheres (2% solid, 200 nm diameter; Invitrogen), 1 μl of 10% (w/v) ammonium persulfate (GE Healthcare), and 1 μl of N,N,N,N-tetramethyl ethylenediamine (Nacalai Tesque) were added to initiate polymerization. Twenty-five μl of the mixture was immediately pipetted onto 18-mm glass coverslips (No. 1, Matsunami) and the previously treated glass bottom dishes were placed, inverted, on the coverslips. After polymerization, the glass coverslips were peeled off and the surfaces of the gels were covered with H_2O to prevent drying until use. Sulfo-SANPAH (1 mM; Pierce) was dropped onto the gels, which were then exposed to UV light under sterile conditions for 5 min, and washed three times with 0.1 M HEPES (pH 7.5) for 15 min. The gel surfaces were coated with 0.1 mg/ml poly-D-lysine (Sigma)

overnight, anti-FC antibody (Jackson) for 3 h, and finally with L1-CAM-FC overnight.

The stiffness of the polyacrylamide gels was determined using a microsphere indentation method [12]. Briefly, a steel ball (0.6 mm diameter, 7.87 g/cm^3; Sato Tekkou) was placed on the gels embedded with fluorescent beads. The indentation caused by the steel ball was measured using a microscope. Young's modulus was obtained as $E = 3(1-v^2)f/4d^{3/2}r^{1/2}$, where f is the buoyancy-corrected weight of the steel ball, d is the indentation of the gel, r is the radius of the steel ball, and v is the Poisson's ratio (whose value is 0.3, as determined previously [45]). The Young's modulus was 269.42 ± 24.17 N/m^2 (mean ± SE, n = 7).

Time-lapse imaging of fluorescent beads and growth cones was performed at 37°C using a confocal microscope (LSM700 or LSM710; Carl Zeiss) equipped with a plan-Apochromat 63x 1.40 oil M27 objective. The growth cone area was determined from EGFP fluorescence or DIC images. In all analyses, we measured bead displacement under the peripheral domain (including filopodia and lamellipodia) and the central domain of axonal growth cones but not under the axonal shaft. After observation, the glass bottom dishes were treated with 1% SDS to release neurons from the polyacrylamide gel substrate, and an image of the unstrained substrate was acquired.

To detect bead location at axonal growth cones in data images and remove noise automatically, we introduced a computational algorithm based on the assumption of sparse bead distribution ("dantzig selector") [46], in which the bead image was expressed as a weighted linear summation of 2D Gaussians with a fixed size. The weight and size of Gaussians correspond to the fluorescence intensity and diameter, respectively. Individual beads were tracked through the time-lapse images, by identifying beads which minimized the sum of the differences in both location and fluorescence intensities with the beads in the reference image. Drifts of bead images during time-lapse observation were offset by minimizing the translocations of beads outside the borders of cells between data images and the reference image, which was obtained after neurons were removed at the end of the experiments. Traction force was estimated from the bead displacements based on an algorithm reported previously [47]. Briefly, if the bead is initially located at $\mathbf{x} = [x, y]$, bead displacement by the force $\mathbf{f}(\mathbf{x})$ can be formulated by $\mathbf{u}(\mathbf{x}) = \int_\Omega G(\mathbf{x}-\mathbf{x}')\,\mathbf{f}(\mathbf{x})\mathrm{d}\mathbf{x}$ with the Green function $G(\mathbf{x}) = \frac{1+\nu}{\pi E r^3}\begin{bmatrix}(1-\nu)r^2+\nu x^2 & \nu xy \\ \nu xy & (1-\nu)r^2+\nu y^2\end{bmatrix}$, where ν and E are the Poisson ratio (0.3) and Young's modulus (269.42 N/m^2), respectively, and $r = |\mathbf{x}|$.

Using the bead displacement dataset, the force was reversely computed from this integral formulation. The force per unit area (Pa) was calculated by dividing the estimated force by the area of the single pixel of the growth cone image ($(9.62 \times 10^{-8})^2 \mathrm{m}^2$). The net force in Fig. 1D represents the summation of all the estimated force vectors under the growth cone.

Cell surface biotinylation assays of L1-CAM

Biotinylation of extracellular L1-CAM was carried out as described previously [48]. Briefly, DIV2 cultured neurons were washed with ice-cold Ca/Mg-PBS (PBS containing 1 mM $MgCl_2$ and 0.1 mM $CaCl_2$) and incubated with 2.5 mg/ml EZ-Link Sulfo-NHS-LC-biotin (Pierce) in Ca/Mg-PBS for 30 min at 4°C. The reaction was quenched with 50 mM glycine in Ca/Mg-PBS. The cells were then lysed in lysis buffer (PBS containing 1% Triton X-100, 0.1% SDS, 0.5% deoxycholate, 2 mM PMSF, and 2 mg/ml leupeptin). After centrifugation for 15 min at 17,400 g, the supernatant was incubated with streptavidin-agarose beads (Pierce) for 2 h at 4°C. Bound proteins were immunoblotted with anti-L1-CAM antibody (C-20, Santa Cruz).

Statistical analysis

Significance was determined by one-way ANOVA for multiple comparisons, Student's *t*-test for a single comparison with Gaussian distribution, or the Mann-Whitney *U* test for a single comparison with non-Gaussian distribution, using GraphPad INSTAT software version 3.10 (GraphPad).

Supplemental References

1. Pollard, T.D., and Borisy, G.G. (2003). Cellular motility driven by assembly and disassembly of actin filaments. Cell *112*, 453-465.
2. Le Clainche, C., and Carlier, M.F. (2008). Regulation of actin assembly associated with protrusion and adhesion in cell migration. Physiol. Rev. *88*, 489-513.
3. Forscher, P., and Smith, S.J. (1988). Actions of cytochalasins on the organization of actin filaments and microtubules in a neuronal growth cone. J. Cell Biol. *107*, 1505-1516.
4. Katoh, K., Hammar, K., Smith, P.J., and Oldenbourg, R. (1999). Birefringence imaging directly reveals architectural dynamics of filamentous actin in living growth cones. Mol. Biol. Cell *10*, 197-210.
5. Medeiros, N.A., Burnette, D.T., and Forscher, P. (2006). Myosin II functions in actin-bundle turnover in neuronal growth cones. Nat. Cell Biol. *8*, 215-226.
6. Mitchison, T., and Kirschner, M. (1988). Cytoskeletal dynamics and nerve growth. Neuron *1*, 761-772.
7. Suter, D.M., and Forscher, P. (2000). Substrate-cytoskeletal coupling as a mechanism for the regulation of growth cone motility and guidance. J. Neurobiol. *44*, 97-113.
8. Hu, K., Ji, L., Applegate, K.T., Danuser, G., and Waterman-Storer, C.M. (2007). Differential transmission of actin motion within focal adhesions. Science *315*, 111-115.
9. Giannone, G., Mege, R.M., and Thoumine, O. (2009). Multi-level molecular clutches in motile cell processes. Trends Cell Biol. *19*, 475-486.
10. Lowery, L.A., and Van Vactor, D. (2009). The trip of the tip: understanding the growth cone machinery. Nat. Rev. Mol. Cell Biol. *10*, 332-343.
11. Shimada, T., Toriyama, M., Uemura, K., Kamiguchi, H., Sugiura, T., Watanabe, N., and Inagaki, N. (2008). Shootin1 interacts with actin retrograde flow and L1-CAM to promote axon outgrowth. J. Cell Biol. *181*, 817-829.
12. Chan, C.E., and Odde, D.J. (2008). Traction dynamics of filopodia on compliant substrates. Science *322*, 1687-1691.
13. Koch, D., Rosoff, W.J., Jiang, J., Geller, H.M., and Urbach, J.S. (2012). Strength in the periphery: growth cone biomechanics and substrate rigidity response in peripheral and central nervous system neurons. Biophys. J. *102*, 452-460.
14. Li, X., Gao, X., Liu, G., Xiong, W., Wu, J., and Rao, Y. (2008). Netrin signal transduction and the guanine nucleotide exchange factor DOCK180 in attractive signaling. Nat. Neurosci. *11*, 28-35.

15. Serafini, T., Kennedy, T.E., Galko, M.J., Mirzayan, C., Jessell, T.M., and Tessier-Lavigne, M. (1994). The netrins define a family of axon outgrowth-promoting proteins homologous to C. elegans UNC-6. Cell *78*, 409-424.

16. Shekarabi, M., Moore, S.W., Tritsch, N.X., Morris, S.J., Bouchard, J.F., and Kennedy, T.E. (2005). Deleted in colorectal cancer binding netrin-1 mediates cell substrate adhesion and recruits Cdc42, Rac1, Pak1, and N-WASP into an intracellular signaling complex that promotes growth cone expansion. J. Neurosci. *25*, 3132-3141.

17. Garvalov, B.K., Flynn, K.C., Neukirchen, D., Meyn, L., Teusch, N., Wu, X., Brakebusch, C., Bamburg, J.R., and Bradke, F. (2007). Cdc42 regulates cofilin during the establishment of neuronal polarity. J. Neurosci. *27*, 13117-13129.

18. Moore, S.W., Biais, N., and Sheetz, M.P. (2009). Traction on immobilized netrin-1 is sufficient to reorient axons. Science *325*, 166.

19. Wang, Y.L., and Pelham, R.J., Jr. (1998). Preparation of a flexible, porous polyacrylamide substrate for mechanical studies of cultured cells. Methods Enzymol. *298*, 489-496.

20. Manser, E., Leung, T., Salihuddin, H., Zhao, Z.S., and Lim, L. (1994). A brain serine/threonine protein kinase activated by Cdc42 and Rac1. Nature *367*, 40-46.

21. Toriyama, M., Shimada, T., Kim, K.B., Mitsuba, M., Nomura, E., Katsuta, K., Sakumura, Y., Roepstorff, P., and Inagaki, N. (2006). Shootin1: A protein involved in the organization of an asymmetric signal for neuronal polarization. J. Cell Biol. *175*, 147-157.

22. Jacobs, T., Causeret, F., Nishimura, Y.V., Terao, M., Norman, A., Hoshino, M., and Nikolic, M. (2007). Localized activation of p21-activated kinase controls neuronal polarity and morphology. J. Neurosci. *27*, 8604-8615.

23. Delorme-Walker, V.D., Peterson, J.R., Chernoff, J., Waterman, C.M., Danuser, G., DerMardirossian, C., and Bokoch, G.M. (2011). Pak1 regulates focal adhesion strength, myosin IIA distribution, and actin dynamics to optimize cell migration. J. Cell Biol. *193*, 1289-1303.

24. Watanabe, N., and Mitchison, T.J. (2002). Single-molecule speckle analysis of actin filament turnover in lamellipodia. Science *295*, 1083-1086.

25. Murray, A., Naeem, A., Barnes, S.H., Drescher, U., and Guthrie, S. (2010). Slit and Netrin-1 guide cranial motor axon pathfinding via Rho-kinase, myosin light chain kinase and myosin II. Neural. Dev. *5*, 16.

26. Bokoch, G.M. (2003). Biology of the p21-activated kinases. Annu. Rev. Biochem. *72*, 743-781.

27. Schmidt, A., and Hall, A. (2002). Guanine nucleotide exchange factors for Rho GTPases: turning on the switch. Genes Dev. *16*, 1587-1609.

28. Kaibuchi, K., Kuroda, S., and Amano, M. (1999). Regulation of the cytoskeleton and cell adhesion by the Rho family GTPases in mammalian cells. Annu. Rev. Biochem. *68*, 459-486.

29. Rohatgi, R., Ma, L., Miki, H., Lopez, M., Kirchhausen, T., Takenawa, T., and Kirschner, M.W. (1999). The interaction between N-WASP and the Arp2/3 complex links Cdc42-dependent signals to actin assembly. Cell *97*, 221-231.

30. Miki, H., Yamaguchi, H., Suetsugu, S., and Takenawa, T. (2000). IRSp53 is an essential intermediate between Rac and WAVE in the regulation of membrane ruffling. Nature *408*, 732-735.

31. Peng, J., Wallar, B.J., Flanders, A., Swiatek, P.J., and Alberts, A.S. (2003). Disruption of the Diaphanous-related formin Drf1 gene encoding mDia1 reveals a role for Drf3 as an effector for Cdc42. Curr. Biol. *13*, 534-545.

32. Huber, A.B., Kolodkin, A.L., Ginty, D.D., and Cloutier, J.F. (2003). Signaling at the growth cone: ligand-receptor complexes and the control of axon growth and guidance. Annu. Rev. Neurosci. *26*, 509-563.

33. Round, J., and Stein, E. (2007). Netrin signaling leading to directed growth cone steering. Curr. Opin. Neurobiol. *17*, 15-21.

34. Guilluy, C., Garcia-Mata, R., and Burridge, K. (2011). Rho protein crosstalk: another social network? Trends Cell Biol. *21*, 718-726.

35. Veniere, S., Ampe, C., Vandekerckhove, J., and Lambrechts, A. (2009). The interaction of proline-rich ligands with profilin probed with an enzyme-linked immunosorbent assay. J. Biomol. Screen. *14*, 350-359.

36. Renkawitz, J., Schumann, K., Weber, M., Lammermann, T., Pflicke, H., Piel, M., Polleux, J., Spatz, J.P., and Sixt, M. (2009). Adaptive force transmission in amoeboid cell migration. Nat. Cell Biol. *11*, 1438-1443.

37. Narumiya, S., and Watanabe, N. (2009). Migration without a clutch. Nat. Cell Biol. *11*, 1394-1396.

38. Ohashi, K., Fujiwara, S., Watanabe, T., Kondo, H., Kiuchi, T., Sato, M., and Mizuno, K. (2011). LIM kinase has a dual role in regulating lamellipodium extension by

decelerating the rate of actin retrograde flow and the rate of actin polymerization. J. Biol. Chem. *286*, 36340-33651.

39. Manser, E., Huang, H.Y., Loo, T.H., Chen, X.Q., Dong, J.M., Leung, T., and Lim, L. (1997). Expression of constitutively active alpha-PAK reveals effects of the kinase on actin and focal complexes. Mol. Cell Biol. *17*, 1129-1143.
40. Zhao, Z.S., Manser, E., Chen, X.Q., Chong, C., Leung, T., and Lim, L. (1998). A conserved negative regulatory region in alphaPAK: inhibition of PAK kinases reveals their morphological roles downstream of Cdc42 and Rac1. Mol. Cell Biol. *18*, 2153-2163.
41. Fukata, M., Kuroda, S., Nakagawa, M., Kawajiri, A., Itoh, N., Shoji, I., Matsuura, Y., Yonehara, S., Fujisawa, H., Kikuchi, A., et al. (1999). Cdc42 and Rac1 regulate the interaction of IQGAP1 with beta-catenin. J. Biol. Chem. *274*, 26044-26050.
42. Goto, H., and Inagaki, M. (2007). Production of a site- and phosphorylation state-specific antibody. Nat. Protoc. *2*, 2574-2581.
43. Woodcock, S.A., Jones, R.C., Edmondson, R.D., and Malliri, A. (2009). A modified tandem affinity purification technique identifies that 14-3-3 proteins interact with Tiam1, an interaction which controls Tiam1 stability. J. Proteome Res. *8*, 5629-5641.
44. Bridgman, P.C., Dave, S., Asnes, C.F., Tullio, A.N., and Adelstein, R.S. (2001). Myosin IIB is required for growth cone motility. J. Neurosci. *21*, 6159-6169.
45. Li, Y., Hu, Z., and Li, C. (1993). New method for measuring Poisson's ratio in polymer gels. J. Appl. Polym. Sci. *50*, 1107-1111.
46. Candes, E., and Tao, T. (2007). The Dantzig selector: Statistical estimation when p is much larger than n. Ann Statist *35*, 2313-2351.
47. Sabass, B., Gardel, M.L., Waterman, C.M., and Schwarz, U.S. (2008). High resolution traction force microscopy based on experimental and computational advances. Biophys J *94*, 207-220.
48. Bouchard, J.F., Moore, S.W., Tritsch, N.X., Roux, P.P., Shekarabi, M., Barker, P.A., and Kennedy, T.E. (2004). Protein kinase A activation promotes plasma membrane insertion of DCC from an intracellular pool: A novel mechanism regulating commissural axon extension. J. Neurosci. *24*, 3040-3050.